Journal of Applied Physics

Contact-induced spin polarization in graphene/*h*-BN/Ni nanocomposites

Cite as: J. Appl. Phys. **112**, 114303 (2012); https://doi.org/10.1063/1.4767134
Submitted: 12 July 2012 . Accepted: 26 October 2012 . Published Online: 03 December 2012

Pavel V. Avramov, Alex A. Kuzubov, Seiji Sakai, Manabu Ohtomo, Shiro Entani, Yoshihiro Matsumoto, Hiroshi Naramoto, and Natalia S. Eleseeva

View Online Export Citation CrossMark

ARTICLES YOU MAY BE INTERESTED IN

Contact-induced spin polarization of monolayer hexagonal boron nitride on Ni(111)
Applied Physics Letters **104**, 051604 (2014); https://doi.org/10.1063/1.4863324

Contact-induced spin polarization in BNNT(CNT)/TM (TM=Co, Ni) nanocomposites
Journal of Applied Physics **116**, 084309 (2014); https://doi.org/10.1063/1.4894157

The adsorption of h-BN monolayer on the Ni(111) surface studied by density functional theory calculations with a semiempirical long-range dispersion correction
Journal of Applied Physics **115**, 17C117 (2014); https://doi.org/10.1063/1.4866237

© 2012 American Institute of Physics.

JOURNAL OF APPLIED PHYSICS **112**, 114303 (2012)

Contact-induced spin polarization in graphene/*h*-BN/Ni nanocomposites

Pavel V. Avramov,[1,2,a)] Alex A. Kuzubov,[2] Seiji Sakai,[1] Manabu Ohtomo,[1] Shiro Entani,[1] Yoshihiro Matsumoto,[1] Hiroshi Naramoto,[1] and Natalia S. Eleseeva[2]
[1]*Advanced Science Research Center, Japan Atomic Energy Agency, 2-4 Shirakata Shirane, Tokai-mura, Naka-gun, Ibaraki-ken 319-1195, Japan*
[2]*L.V. Kirensky Institute of Physics SB RAS, Krasnoyarsk 660036, Russia*

(Received 12 July 2012; accepted 26 October 2012; published online 3 December 2012)

Atomic and electronic structure of graphene/Ni(111), *h*-BN/Ni(111) and graphene/*h*-BN/Ni(111) nanocomposites with different numbers of graphene and h-BN layers and in different mutual arrangements of graphene/Ni and *h*-BN/Ni at the interfaces was studied using LDA/PBC/PW technique. Using the same technique corresponding graphene, *h*-BN and graphene/*h*-BN structures without the Ni plate were calculated for the sake of comparison. It was suggested that C-*top*:*C-fcc* and N-*top*:*B-fcc* configurations are energetically favorable for the graphene/Ni and *h*-BN/Ni interfaces, respectively. The Ni plate was found to induce a significant degree of spin polarization in graphene and *h*-BN through exchange interactions of the electronic states located on different fragments. © *2012 American Institute of Physics*. [http://dx.doi.org/10.1063/1.4767134]

I. INTRODUCTION

Organic molecule- and nanocarbon-based spintronics is a very promising technological field because carbon atoms exhibit weak spin–orbit interactions, which enable one to utilize long spin transport together with extremely high mobility of electrons in spintronic devices.[1–3] Spin transport on graphene has been demonstrated using the electrical spin injection from the ferromagnetic support.[4] The atomic and electronic structure of graphene epitaxially grown on the Ni(111) surface has been carefully studied (see, for example, Refs. 5–9) and, particularly, a visible hybridization of graphene π- and Ni 3*d* valence-band states as well as appearance of the induced magnetic moment on the carbon atoms due to C2p_z spin polarization was reported. Among several graphene/Ni(111) interfaces, the *hcp*:*fcc* (carbon atoms are placed under *hcp* and *fcc* positions of the nickel lattice with nickel-graphene distance 2.8 Å) and *top*:*fcc* (2.11 and 2.16 Å for both graphene sublattices) configurations have been reported experimentally.[10,11]

The Perdew-Burke-Ernzerhof periodic boundary conditions (PBC/PBE) calculations of graphene/Ni(111)[12,13] have revealed the *top*:*fcc* as the most stable atomic configuration. The Ni-C distances between Ni layer located at the interface and the adjusted graphene layer were calculated to be 2.122 and 2.130 Å for both graphene sublattices. In the calculations, the spin magnetic moments of the Ni atoms at the interface and the C-*top* and C-*fcc* atoms in graphene were derived to be 0.553 μ_B, $-0.01\,\mu_B$ and $-0.02\,\mu_B$, respectively. The induced magnetic moment of the carbon atoms was attributed to the visible hybridization between graphene π and Ni 3*d* valence-band states and the partial charge transfer of the spin-polarized electrons from Ni onto C. The long-range van der Waals interactions were taken into account[9,14] to calculate atomic and electronic structure of complex graphene/Al/Ni(111) and graphene/Ni(111) interfaces. In particular, it was found that the ferromagnetic support induces a weak ferrimagnetism in graphene with unequal magnetic moments $-0.04\,\mu$B and $+0.06\,\mu$B on nonequivalent graphene carbon atoms.

The x-ray photoelectron diffraction study of epitaxial *h*-BN on the Ni(111) surface revealed a coexistence of the N-*top*:B-*fcc* and N-*top*:B-*hcp* configurations[15] with the distances of 1.88 and 1.95 Å for the B and N atoms from the Ni surface, respectively.[16–18] However, contradictory results have also been reported for the degree of the π-d hybridization at the *h*-BN/Ni(111) interface.[19–22]

Full potential linear augmented plane-wave calculations[23–25] demonstrate the insulating nature of *h*-BN monolayer on the Ni (111) surface. It was found that the energy difference between the N-*top*:B-*fcc* and N-*top*:B-*hcp* configurations is equal to 9 meV. The energy difference between the N-*top*:B-*hcp* and B-*top*:N-*fcc* configurations is smaller and equal to 4.0 meV. At the GGA level of theory, the distances of the B and N atoms from the Ni surface are 2.177 Å and 2.252 Å, respectively, while LDA gives the values of 1.946 Å and 2.051 Å, respectively.

The atomic and electronic structure of the graphene sheet placed on a top of a lattice-matched *h*-BN have been studied both experimentally[26] and theoretically.[27,28] The appearance of Moiré patterns in the experimental study suggests the close (but not equal) lattice parameters in graphene and *h*-BN. In spite of the misalignment of the lattices, only a small band gap (53 meV) was detected in the electronic structure of graphene.

Inserting of chemically inert *h*-BN interlayer between the fragments can protect graphene against the direct chemical interactions with metal substrate. For the graphene/Ni, *h*-BN/Ni and graphene/*h*-BN/Ni nanocomposites, the spectroscopic techniques cannot provide complete and consistent structural data. Moreover, the most technologically promising graphene/*h*-BN/Ni nanocomposites have been still unexplored theoretically. To interpret the experimental spectra and to perform pre-arranged chemical synthesis of the

[a)]Author to whom correspondence should be addressed. Electronic mail: avramov.pavel@jaea.go.jp.

 © 2012 American Institute of Physics

nanocomposites, extensive quantum chemical calculations should be performed. In the present study, the atomic and electronic structure and spin states of graphene/Ni(111), *h*-BN/Ni(111) and graphene/*h*-BN/Ni(111) nanocomposites with different numbers of graphene and *h*-BN layers, and in different mutual arrangements at the graphene/*h*-BN, graphene/Ni and *h*-BN/Ni interfaces were studied by means of PBC version of plane wave (PW) LDA technique. The 2D nanocomposites were designed by consequent addition of graphene and *h*-BN layers on the (111) surface of the *fcc* 9 layer Ni plate. The LDA calculations reveal *top*:*fcc* type of graphene/Ni and *h*-BN/Ni interfaces as the most energetically favorable structures. A small charge transfer from the Ni plate to the first graphene and *h*-BN layers is also evaluated. The creation of the graphene/*h*-BN/Ni nanocomposites leads to the spin polarization of electronic states localized on both graphene and *h*-BN fragments due to the direct exchange interactions with the electronic states localized on the Ni sites.

II. METHOD OF CALCULATIONS AND 2D NANOCOMPOSITE STRUCTURE MODELS

The atomic and electronic structures of a set of graphene, *h*-BN, graphene/*h*-BN, graphene/Ni, *h*-BN/Ni, and graphene/*h*-BN/Ni with different numbers of graphene and *h*-BN layers were calculated in different configurations. In order to calculate the atomic and electronic structure of 2D nanocomposites, the LDA approximation, PW basis sets and ultrasoft Vanderbilt-type pseudopotentials (PP) in PBC were used. For all calculations the cutoff energy (E_{cutoff}) is equal to 286 eV. The VASP code[29,30] was employed to perform electronic structure calculations. The geometry of the structures was optimized until residual forces became less than 0.01 eV/Å. The Γ-centered Monkhorst-Pack[31] (10×10×01) *k*-point Brillouin zone sampling scheme was used.

The pristine Ni plate with two equivalent *fcc* (111) surfaces contained nine atomic layers (five nonequivalent ones) was calculated as the reference structure. Structural parameters of all 2D nanocomposites including the Ni plate are presented in Tables I–V. An example of the nanocomposite with two fragments (a graphene sheet on the Ni plate in *top*:*fcc* configuration) is presented in Fig. 1. To reproduce the symmetry restrictions of Ni *fcc* crystal properly, the rectangular supercell with 18 Ni atoms (each single atomic layer provides two Ni atoms) was employed. The translational vectors *a* and *b*, which reflect the basis of the rectangle (equivalent to the Ni-Ni interatomic distances) and the length of the rectangle, were equal to 2.444 and 4.226 Å, respectively. The Ni-Ni interlayer distances were in the range of 1.963-1.995 Å depending the position of the layers with respect to the plate surfaces. To avoid interaction of the partner structures, multiplied by PBC algorithm in *z* direction, the length of *c* translation vector was equal to 40.8 Å.

The supercells of the graphene/Ni, *h*-BN/Ni and graphene/*h*-BN/Ni nanocomposites were designed as superposition of the graphene, *h*-BN and Ni plate supercells. The numbers of the graphene and *h*-BN layers in the nanocomposites were varied in the range of $L = 1$-4 and $N = 1$-3, respectively. The *top*:*fcc* configurations of graphene/Ni and *h*-BN/Ni interfaces (namely, N-*top*:B-*fcc*, N-*top*:B-*hcp*, B-*top*:N-*fcc*, and B-*top*:N-*hcp* ones) were used to calculate the electronic structure of all nanocomposites (Tables II, III, and V). The AB configuration of the graphene sheets was employed to calculate the electronic structure of the nanocomposites made of multilayer graphene ($L > 1$). The lowest in energy (AA′) and (AB′) configurations of neighboring *h*-BN layers was used to study the electronic structure of the *h*-BN-based nanocomposites. For the sake of comparison, all possible multilayer graphene, multilayer *h*-BN ($L, N > 1$), and multilayer graphene/multilayer *h*-BN-based nanocomposites were calculated in (AB), (ABC), and (AA). The multilayer graphene and multilayer *h*-BN unit cells contain $2 \times L + 2 \times N$ atoms. For graphene, both *a* and *b* translational vectors were equal to 2.438 Å with C-C distances equal to 1.408 Å. The graphene-graphene interlayer distances for multilayer

TABLE I. Details of atomic and electronic structures of the graphene, *h*-BN, and Ni plate.

	Atom-atom distances (Å)	Type of configuration	Interlayer distances (Å)	Interlayer binding energy E_{bind}/*unit cell*/*layer* (eV)	Total atomic spin density (atomic charge of external Ni atoms (spin)
Monolayer graphene (C-C)	1.408	…	…	…	…
Bilayer graphene (C-C)	1.408	AB	3.294	−0.0281	…
Trilayer graphene (C-C)	1.408	ABA	3.308	−0.0354	…
Trilayer graphene (C-C)	1.408	ABC	3.281	−0.0370	…
Tetralayer graphene (C-C)	1.408	ABAB	3.304	−0.0400	…
Graphite (C-C)	1.408	AB	3.284	−0.0699	
Monolayer *h*-BN (B-N)	1.430	…	…	…	…
Bilayer *h*-BN (B-N)	1.430	AA′	3.258	−0.0283	…
Bilayer *h*-BN (B-N)	1.430	AB	3.225	−0.0267	…
Trilayer *h*-BN (B-N)	1.430	AA′	3.237	−0.0363	…
Trilayer *h*-BN (B-N)	1.430	ABA	3.236	−0.0376	…
Trilayer *h*-BN (B-N)	1.430	ABC	3.236	−0.0364	…
Ni plate (Ni-Ni)	2.427 – 2.442	*fcc* lattice	1.963–1.995	…	0.613 (0.116)

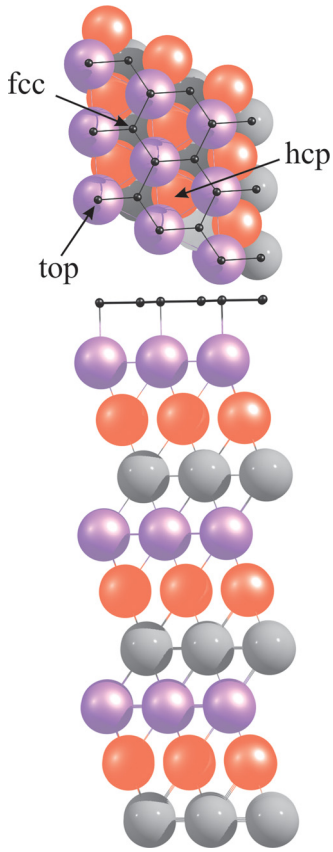

FIG. 1. The schematics of the graphene/Ni nanocomposite. The *top* Ni positions are presented in lilac, and the *hcp* and *fcc* ones are presented in light red and gray, respectively. The carbon atoms of graphene lattice are presented in black.

graphenes were equal to 3.284–3.308 Å. For *h*-BN, both *a* and *b* vectors were equal to 2.476 Å with B-N distances of 1.430 Å. The *h*-BN-*h*-BN, graphene-*h*-BN, and graphene-graphene interlayer distances for the graphene/*h*-BN/Ni nanocomposites were equal to 3.148–3.217 Å, 3.125–3.307 Å, and 3.255–3.37 Å, respectively.

III. RESULTS AND DISCUSSION

The details of atomic structure of multilayered graphenes and *h*-BNs and Ni plate as well are summarized in Table I. Tables II–V represent the atomic structures of the graphene/Ni, *h*-BN/Ni, graphene/*h*-BN, and graphene/*h*-BN/Ni nanocomposites, respectively. The graphite structure was calculated for the sake of comparison, and the structural data (1.408 Å C-C bond length and 3.284 Å interlayer distance) were confirmed to be coincident with experimental results (1.422 ± 0.001 Å and 3.356 ± 0.002 Å, respectively).[32] The graphene carbon-carbon bond lengths were reproduced by LDA/PW/PP/PBC with the same accuracy. For bilayer, trilayer, and tetralayer graphenes, the interlayer distances were equal to 3.294, 3.308, and 3.304 Å, respectively. The increase of the number of graphene layers leads to the increase of graphene-graphene bond energy from − 0.0281 up to −0.0400 eV/unit cell approaching to the limit of graphite (−0.0699 eV/unit cell). For trilayer graphene, ABA and ABC configurations were calculated, and close binding energies per unit cell were obtained (0.0354 and 0.0370 eV/unit cell, respectively, Table I). It is necessary to note that the trilayer graphene exhibit both ABA[33,34] and ABC[35] crystallographic stacking. At the *ab initio* HSE/6-21 G and 6-21 G* PBC calculations, the ABC configuration is energetically favorable, whereas the ABA stacking is energetically favorable in the case of medium basis sets (6-31 G and 6-31 G*).[36]

The LDA/PW/PP/PBC slightly underestimates the B-N bond length (1.430 Å, Table I, experimental value 1.443 Å (Refs. 37 and 38). For bilayer *h*-BN, the LDA PW PP PBC gives the same B-N distance (1.430 Å) with a very small (0.0016 eV) energy difference between AA′ and AB configurations and 3.225 and 3.258 Å interlayer distances between *h*-BN layers, respectively (experimental value is equal to 3.33 Å (Refs. 38 and 39). Trilayer *h*-BN with the AA′, ABA, and ABC configurations shows much smaller energy difference (0.0001–0.0012 eV, Table I) than the accuracy of the method with practically the same values of interlayer distances (3.236-3.237 Å). The LDA/PW/PP/PBC calculations of the Ni plate demonstrate reasonable performance in reproduction of Ni-Ni bond length (2.427-2.442 Å, Table I) in comparison with experimental data (2.492 Å).[40] The underestimation of the Ni-Ni bond lengths in our calculations is caused by replacing of the bulk Ni structure by relatively thick Ni plate with two unsaturated surfaces. Redistribution of valence electrons from dangling bonds among all atoms of the plate leads to the increase of the binding energy and consequent decrease of the lengths of Ni-Ni bonds.

The details of atomic structure of a *top*:*fcc* coordinated graphene/Ni nanocomposite are presented in Fig. 1 and Table II. The *top*:*fcc* configuration is energetically favorable, and the binding energy is equal to −0.0465 eV/unit cell in

TABLE II. Atomic and electronic structures of the graphene/Ni nanocomposites. Monolayer graphene/Ni, bilayer graphene/Ni, trilayer graphene/Ni, and tetralayer graphene/Ni were calculated in the *top*:*fcc* and AB configurations of graphene/Ni and graphene/graphene interfaces, respectively.

	min Ni-Ni/C-C distances (Å)	*max* Ni-Ni/C-C distances (Å)	Ni-C distance (Å)	graphene–Ni plate distance (Å)	graphene-graphene distances (Å)	graphene–Ni plate binding energy (eV/cell)	Energy of adding of consequent graphene layer (eV/cell)
Monolayer graphene/Ni *top*:*fcc*	1.951/1.410	1.973/1.410	2.064	2.064	…	−0.0465	…
Monolayer graphene/Ni *fcc*:*hcp*	1.961/1.410	1.983/1.410	3.900	3.617	…	−0.0385	…
Bilayer graphene/Ni	1.952/1.410	1.975/1.410	2.063	2.063	3.008	−0.2134	−0.0455
Trilayer graphene/Ni	1.949/1.410	1.976/1.410	2.061	2.061	3.290/3.289	−0.2474	−0.0627
Tetralayer graphene/Ni	1.956/1.410	1.974/1.410	2.076	2.076	3.312/3.306/3.305	−0.2712	−0.0618

TABLE III. Atomic and electronic structures of the *h*-BN/Ni nanocomposites. For N-*top*:B-*fcc* configurations, the maximal Ni-Ni distances are observed at the *h*-BN/Ni interface, while the smallest ones are located at the opposite side of the plane. In the case of bilayer and trilayer *h*-BN, the longest B-N bonds belong to the interface *h*-BN layer, while the shortest ones are located in the top *h*-BN layer.

	Type of configuration	*min* Ni-Ni/B-N distances (Å)	*max* Ni-Ni/B-N distances (Å)	*h*-BN–Ni plate distance (Å)	*h*-BN–*h*-BN distances (Å)	*h*-BN–Ni plate binding energy (eV/cell)	Energy of adding of *h*-BN sheet (eV/cell)
Monolayer *h*-BN/Ni	N-*top*:B-*fcc*	2.407/1.417	2.428/1.417	2.085	…	−0.1335	…
Monolayer *h*-BN/Ni	N-*top*:B-*hcp*	2.406/1.417	2.429/1.417	2.090	…	−0.1230	…
Monolayer *h*-BN/Ni	B-*top*:N-*fcc*	2.408/1.405	2.431/1.405	3.168	…	0.0524	…
Monolayer *h*-BN/Ni	B-*top*:N-*hcp*	2.410/1.403	2.430/1.403	3.086	…	0.1556	…
Bilayer *h*-BN/Ni	N-*top*:B-*fcc* B-*top:N-hcp*	2.406/1.413	2.428/1.417	2.084	3.122	−0.1137	−0.0369
Bilayer *h*-BN/Ni	N-*top*:B-*fcc* B-*top:N-fcc*	2.406/1.413	2.428/1.417	2.084	3.223	−0.1130	−0.0362
Billayer *h*-BN/Ni	N-*top*:B-*fcc* B-*hcp:N-fcc*	2.405/1.412	2.427/1.417	2.083	3.226	−0.1120	−0.0353
Trilayer *h*-BN/Ni	N-*top*:B-*fcc* B-*hcp:N-fcc* B-*top:N-hcp*	2.405/1.412	2.425/1.417	2.079	3.228 3.221	−0.2038	−0.0351
Trilayer *h*-BN/Ni	N-*top*:B-*fcc* B-*top:N-hcp N-top*:B-*fcc*	2.407/1.413	2.437/1.417	2.063	3.235 3.145	−0.1550	0.0153

comparison with −0.0385 eV/unit cell for the *fcc*:*hcp* configuration. Because of that, the structural and electronic data for the *fcc*:*hcp* configurations are omitted in the present work.

For the *top*:*fcc* configuration, the graphene-Ni interlayer distance is equivalent to the Ni-C bond length and equal to 2.064 Å (Table II). The Ni-C bond length for the *fcc*:*hcp* configuration is much larger and amounts to 3.900 Å with the graphene-Ni interlayer distance of 3.617 Å. Formation of the graphene/Ni nanocomposites leads to the consequent increase of the binding energy of graphene and Ni plate (from −0.0465 eV/unit cell for monolayer graphene/Ni up to −0.2712 eV/unit cell for tetralayer graphene/Ni) and consequent slight decrease of the graphene-graphene interlayer distances. In all cases, the ABA configuration of the graphene layers is energetically favorable.

The details of atomic structure of *h*-BN/Ni nanocomposites are presented in Table III. The N-*top*:B-*fcc* configuration is energetically favorable, and the N-*top*:B-*hcp* configuration is a metastable structure. Meanwhile, both B-*top*:N-*fcc* and B-*top*:N-*hcp* configurations are unstable. For the N-*top*:B-*fcc* configurations, the maximal Ni-Ni distances are observed at the *h*-BN/Ni interface, while the smallest ones are located at the opposite side of the plane. In the case of bilayer and trilayer *h*-BNs, the longest B-N bonds are located at the interface *h*-BN layer, while the shortest ones are located at the top *h*-BN layer of the multilayer complex. For the stable and metastable N-*top*:B-*fcc* and N-*top*:B-*hcp* configurations, the chemical bond nature of the interface *h*-BN layer is determined by direct N-Ni interactions, so the number of the *h*-BN layers in the composites slightly affects the (*h*-BN)-Ni interlayer distance: the increase of the layer number slightly decreases the interlayer distance (Table III). For the stable *h*-BN configurations, an additional *h*-BN layers increases binding energy of *h*-BN and Ni fragments.

The details of atomic structure of graphene/*h*-BN nanocomposites are presented in Table IV. Since the unit cell of the composites is the same as that for both fragments, the C-C and B-N bond lengths were equal to 1.419 Å for all calculations. For the graphene/*h*-BN structure, the B-*top* is energetically favorable configuration among three possible ones (B-*top*, N-*top*, and N-*top*:B-*top*) with the shortest graphene-*h*-BN interlayer distance equal to 3.221 Å. The bilayer graphene/bilayer *h*-BN nanocomposites show close stability of two possible B-*top* AA-, AB(C)-, and $A_1B(A_2)$-type configurations of graphene and *h*-BN fragments. All N-*top* configurations are less stable than the B-*top* ones.

The details of atomic structure of the graphene/*h*-BN/Ni nanocomposites with different numbers of graphene and

TABLE IV. Details of atomic structures of the graphene/*h*-BN structures.

	graphene-graphene type of configuration	*h*-BN–*h*-BN type of configuration	graphene–*h*-BN type of configuration	Interlayer distances (*h*-BN–*h*-BN)/(graphene–*h*-BN)/(graphene–graphene) (Å)	Interlayer binding energies (*h*-BN–*h*-BN)/(graphene–*h*-BN)/(graphene–graphene) (eV)
Monolayer graphene/monolayer *h*-BN	…	…	B-*top*	(…)/(3.221)/(…)	(…)/(−0.0469)/(…)
Monolayer graphene/monolayer *h*-BN	…	…	N-*top*	(…)/(3.451)/(…)	(…)/(−0.0281)/(…)
Monolayer graphene/monolayer *h*-BN	…	…	N-*top*:B-*top*	(…)/(3.413)/(…)	(…)/(−0.0240)/(…)
Bilayer graphene/bilayer *h*-BN	AB	AB(C)	B-*top*	(3.397)/(3.349)/(3.363)	(−0.9835)/(−0.0292)/(0.8827)
Bilayer graphene/bilayer *h*-BN	AB	$A_1B(A_2)$	B-*top*	(3.323)/(3.417)/(3.346)	(−0.9764)/(−0.0288)/(0.8831)
Bilayer graphene/bilayer *h*-BN	AB	AB	N-*top*	(3.301)/(3.516)/(3.349)	(−0.9803)/(−0.0148)/(0.8789)
Bilayer graphene/bilayer *h*-BN	AB	AB(C)	B-*top*:N-*top*	(3.287)/(3.544)/(3.264)	(−0.9807)/(−0.0129)/(0.8783)
Bilayer graphene/bilayer *h*-BN	AB	$AB(A_2)$	B-*top*:N-*top*	(3.249)/(3.506)/(3.334)	(−0.9802)/(−0.0127)/(0.8785)
Bilayer graphene/bilayer *h*-BN	AB	AA	B-*top*	(3.478)/(3.429)/(3.348)	(−0.9773)/(−0.0264)/(0.8889)
Bilayer graphene/bilayer *h*-BN	AB	AA	N-*top*	(3.290)/(3.581)/(3.342)	(−0.9806)/(−0.0157)/(0.8810)
Bilayer graphene/bilayer *h*-BN	AB	AA	B-*top*:N-*top*	(3.292)/(3.545)/(3.333)	(−0.9806)/(−0.0143)/(0.8803)

TABLE V. Atomic and electronic structures of the graphene/*h*-BN/Ni nanocomposites. The smallest Ni-Ni distances are located at the non-bonded side of the Ni plate. In the case of bilayer and trilayer *h*-BN, the longest B-N bonds belong to the interface *h*-BN layer.

	Type of configuration	*min* Ni-Ni/ B-N/C-C distances (Å)	*max* Ni-Ni/ B-N/C-C distances (Å)	*h*-BN–Ni plate distance (Å)	*h*-BN–*h*-BN distance (Å)	graphene–graphene distance (Å)	graphene–*h*-BN distance (Å)	graphene/ *h*-BN–Ni plate fragment binding energy[a] (eV/cell)
Monolayer graphene/ monolayer *h*-BN/Ni	N-*top*:B-*fcc* C-*fcc*:C-*hcp*	2.406/1.416/1.412	2.428/1.416/1.412	2.080	…	…	3.205	−0.2075(−0.1607)
Monolayer graphene/ bilayer *h*-BN/Ni	N-*top*:B-*fcc* B-*top*:N-*hcp* C-*top*:C-*fcc*	2.405/1.413/1.414	2.431/1.416/1.414	2.090	3.298	…	3.236	−0.1774(−0.1433)
Monolayer graphene/ bilayer *h*-BN/Ni	N-*top*:B-*fcc* B-*hcp*:N-*fcc* C-*top*:C-*hcp*	2.405/1.412/1.413	2.423/1.416/1.413	2.075	3.148	…	3.126	−0.1803(−0.1529)
Monolayer graphene/ bilayer *h*-BN/Ni	N-*top*:B-*fcc* B-*top*:N-*fcc* C-*top*:C-*hcp*	2.406/1.413/1.414	2.428/1.416/1.414	2.082	3.194	…	3.222	−0.1816(−0.1542)
Bilayer graphene/ bilayer *h*-BN/Ni	N-*top*:B-*fcc* B-*hcp*:N-*fcc* C-*top*:C-*hcp* C-*top*:C-*fcc*	2.403/1.414/1.412	2.424/1.414/1.413	2.075	3.149	3.255	3.125	−0.1852(−0.1560)
Bilayer graphene/ bilayer *h*-BN/Ni	N-*top*:B-*fcc* B-*top*:N-*hcp* C-*top*:C-*fcc* C-*hcp*:C-*fcc*	2.406/1.413/1.413	2.429/1.417/1.414	2.086	3.217	3.320	5.203	−0.1274(−0.0985)
Bilayer graphene/ bilayer *h*-BN/Ni	N-*top*:B-*fcc* B-*top*:N-*fcc* C-*top*:C-*hcp* C-*top*:C-*fcc*	2.406/1.414/1.413	2.438/1.417/1.414	2.067	3.201	3.370	3.307	−0.0512(−0.0282)

[a]Total binding energy (Ni-conglomerate binding energy).

h-BN layers are presented in Table V. As in the case of the *h*-BN/Ni nanocomposites, the shortest Ni-Ni bonds are located at the non-bonded side of the Ni plate. In the case of bilayer and trilayer *h*-BNs, the longest B-N bonds can be found at the *h*-BN/Ni interface. The (*h*-BN)-Ni and (*h*-BN)-(*h*-BN) interlayer distances for all nanocomposites are close to 2.08 and 3.2 Å, respectively. The latter value coincides well with the results for the *h*-BN/Ni (Table III) and *h*-BN (Table I) calculations and slightly smaller than that for graphene/*h*-BN (Table IV). The monolayer graphene/monolayer *h*-BN/Ni nanocomposite has the highest (graphene/*h*-BN)-Ni binding energy among all samples. Excluding one AA-type configuration of *h*-BN (N-*top*:B-*fcc;* B-*top*:N-*fcc*), the energy difference between the samples is close to or less than the accuracy of the LDA PP PW approach. The graphene-*h*-BN binding energies of the most stable structures are also close to each other and coincide with the data for the graphene/*h*-BN structures.

Formation of the graphene/Ni nanocomposite leads to significant decrease of the total atomic spin densities of the first Ni layer atoms from 0.613 (Ni plate, Table I) to 0.4606 (graphene/Ni *top*:*fcc,* Table VI) spins. For the *top*:*fcc*

TABLE VI. Partial atomic spin densities and (atomic charges) of the graphene/Ni nanocomposites. Bilayer graphene/Ni, Trilayer graphene/Ni, and Tetralayer graphene/Ni were calculated in the *top*:*fcc* and AB configurations of graphene/Ni plate and graphene/graphene configurations, respectively. The details of atomic structure of the composites are presented in Table II.

	Ni *top*	Ni-*fcc*	Ni *hcp*	Ni back	1C-*top*	1C-*fcc*	1C-*hcp*	2C-*hcp*	2C-*fcc*	3C-*top*	3C-*fcc*	4C-*hcp*	4C-*fcc*
Monolayer graphene/Ni *top*:*fcc*	0.4606 (0.1195)	0.5421 (0.0035)	0.5102 (0.0166)	0.5991 (−0.0239)	−0.0016 (0.0308)	0.0254 (−0.1684)	…	…	…	…	…	…	…
Monolayer graphene/Ni *hcp*:*fcc*	0.5301 (0.0132)	0.5699 (−0.0010)	0.6071 (0.0239)	0.5974 (−0.0272)	…	−0.0042 (0.4291)	−0.0079 (−0.4655)	…	…	…	…	…	…
Bilayer graphene/Ni	0.46593 (0.1173)	0.5490 (0.0082)	0.5121 (0.0057)	0.5812 (−0.0288)	−0.00009 (0.0445)	0.0202 (−0.1584)	…	−0.0052 (0.4435)	−0.0042 (−0.4591)	…	…	…	…
Trilayer graphene/Ni	… (0.1143)	0.5514 (0.0094)	0.4684 (0.0019)	0.5890 (−0.0292)	−0.0072 (0.0467)	−0.0011 (−0.1593)	…	−0.0005 (−0.4514)	0.0006 (0.4398)	0.0003 (0.4486)	−0.0005 (−0.4503)	…	…
Tetralayer graphene/Ni	0.4685 (0.1191)	0.5460 (0.0057)	0.5114 (0.0025)	0.5968 (−0.0304)	−0.0010 (0.0455)	0.0267 (−0.1569)	…	−0.0012 (0.4396)	−0.0037 (−0.4566)	−0.0012 (0.4446)	−0.0084 (−0.4444)	0.0053 (0.4462)	0.0091 (−0.4456)

configuration of all nanocomposites, the formation of graphene/Ni interface leads to an appearance of small negative spin polarization as well as small positive atomic charges in the *top*-coordinated carbon atoms, whereas the *fcc* ones display considerable positive spin densities (0.02–0.03 spins) and large negative atomic charges (from −0.168 up to −0.157 electron charges). Accordingly, it can be said that the total spin polarization of the first graphene layer is predominantly caused by the carbon atoms of the *fcc*-coordinated sublattice coupled with effective spin transfer from the first Ni layer atoms. It is also noteworthy that the second graphene layer of the graphene/Ni nanocomposites with the *top*:*fcc* configuration shows a spin polarization with different sign. The spin density is negative, about −0.004 spins per carbon atom.

Formation of the *h*-BN/Ni nanocomposites also leads to the decrease of the total atomic spin density of the first Ni layer on the interface from 0.613 (Ni plate, Table I) to 0.500 (*h*-BN/Ni N-*top*:B-*hcp*, Table VII) spins. In case of the N-*top* configurations, the formation of the interface gives rise to a considerable degree of positive spin polarization of the first *h*-BN layer. On the other hand, the B-*top* configuration causes only a small negative spin polarization of the *h*-BN fragment.

In the most complicated case of the graphene/*h*-BN/Ni nanocomposites (Table VIII), the spin polarization and atomic charges of the first Ni layer atoms and *h*-BN layers are close to ones for the *h*-BN/Ni nanocomposites. The upper graphene layers does not influence the spin and charge states of the inner (*h*-BN and Ni) fragments of the composites. Analysis of spin polarization of the graphene fragments of graphene/Ni (Table VI) and the graphene/*h*-BN/Ni nanocomposites demonstrates the comparable magnitudes of spin polarization of the carbon atoms even in the absence of direct chemical interactions between graphene-Ni and graphene-*h*-BN fragments. The graphene/h-BN/Ni nanocomposite with one-layered graphene and *h*-BN fragments demonstrates the same signs of spin polarization of *top*- and *fcc*-coordinated carbon atoms, whereas an insertion of the second *h*-BN layers changes the polarization sign of the *fcc*-ones.

The total and partial density of states of non-polarized monolayer and bilayer graphene, *h*-BN, graphene/*h*-BN, and bilayer graphene/bilayer *h*-BN (Figure 2) were used as a reference data to analyze the nature of chemical bonding and spin polarization of the graphene/Ni, *h*-BN/Ni, and graphene/*h*-BN/Ni nanocomposites. At LDA PBC level of theory, monolayer and multilayer graphenes are zero-band gap semiconductors. The forbidden band gaps of monolayer *h*-BN and bilayer *h*-BN are equal to 4.31 and 4.64 eV, respectively. And finally, the total density of states (TDOS) of graphene/*h*-BN is determined by the superposition of the *h*-BN and graphene fragments. This result is perfectly coinside with the experimental observation of transport properties of *h*-BN/graphene composites.[41,42]

Figs. 3(a) and 3(b) show typical density of states of the monolayer graphene/Ni (*top*:*fcc* configuration), bilayer graphene/Ni (*top*:*fcc*), monolayer *h*-BN/Ni (N-*top*:B-*fcc*), and bilayer *h*-BN/Ni (N-*top*:B-*fcc*/*AB*) nanocomposites. The Ni fragment makes the main contribution to the TDOS of the composites. The formation of the interfaces leads to a strong spin polarization of the graphene and *h*-BN density of states in connection with the energy splitting of the spin-up and spin-down states in the Ni plate and due to the direct chemical interactions of Ni and graphene or *h*-BN electronic states. In the case of graphene/Ni, both spin-up and spin-down electrons of graphene near the Fermi level interact with the electronic states of the first Ni layer. For the multilayer graphene/Ni nanocomposites, the relative weight of the hybridized states is much smaller due to superposition of the electronic states of several graphene layers. In opposite to the graphene/Ni nanocomposites, the shapes of spin-up and spin-down densities of *h*-BN fragments are practically the same with the energy splitting of 0.65 eV between them.

TABLE VII. Partial atomic spin densities and (atomic charges) of the *h*-BN/Ni nanocomposites. The details of atomic structure of the composites are presented in Table III.

	Type of configuration	Ni *top*	Ni *fcc*	Ni *hcp*	Ni back	First h-BN	Second *h*-BN	Third *h*-BN
Monolayer *h*-BN/Ni	N-*top*:B-*fcc*	0.5117 (0.0359)	0.5519 (−0.0042)	0.5449 (0.0151)	0.5971 (−0.0275)	0.0186 (−0.0457)	…	…
Monolayer *h*-BN/Ni	N-*top*:B-*hcp*	0.4997 (0.0296)	0.5523 (−0.0013)	0.6013 (0.0132)	0.6013 (−0.0283)	0.0122 (−0.0402)	…	…
Monolayer *h*-BN/Ni	B-*top*:N-*fcc*	0.5715 (−0.0293)	0.5625 (−0.0004)	0.6027 (0.0282)	0.5492 (−0.0309)	−0.0015 (0.0019)	…	…
Monolayer *h*-BN/Ni	B-*top*:N-*hcp*	0.5652 (−0.0172)	0.5578 (−0.0042)	0.6017 (0.0247)	0.5913 (−0.0216)	−0.0020 (−0.0039)	…	…
Bilayer *h*-BN/Ni	N-*top*:B-*fcc* B-*top*:*N-hcp*	0.5058 (0.0346)	0.5493 (−0.0025)	0.5305 (0.0129)	0.6002 (−0.0229)	0.0107 (−0.0403)	0.0005 (−0.0036)	…
Bilayer *h*-BN/Ni	N-*top*:B-*fcc* B-*top*:*N-fcc*	0.5072 (0.0347)	0.5489 (−0.0029)	0.5297 (0.0128)	0.5547 (−0.0236)	0.0114 (−0.0417)	0.0012 (−0.0020)	…
Bilayer *h*-BN/Ni	N-*top*:B-*fcc* B-*hcp*:*N-fcc*	0.5074 (0.0322)	0.5489 (0.0021)	0.5292 (0.0084)	0.5987 (−0.0194)	0.0117 (−0.0438)	0.0020 (0.0025)	…
Trilayer *h*-BN/Ni	N-*top*:B-*fcc* B-*hcp*:*N-fcc* B-*top*:*N-hcp*	0.5021 (0.0454)	0.5507 (−0.0025)	0.5265 (0.0080)	0.6007 (−0.0291)	0.0123 (−0.0468)	0.0008 (*0.0031)	−0.0041 (0.0016)
Trilayer *h*-BN/Ni	N-*top*:B-*fcc* B-*top*:*N-hcp* *N-top:* B-*fcc*	0.5121 (0.0311)	0.5512 (0.0019)	0.5310 (0.0085)	0.6087 (−0.0308)	0.0133 (−0.0379)	−0.0005 (−0.0029)	−0.0097 (−0.0002)

TABLE VIII. Partial layer spin densities and (layer charges) of the graphene/*h*-BN/Ni nanocomposites. The details of atomic structure of the composites are presented in Table V.

	Type of *h*-BN configuration	Type of graphene configuration	Ni *top*	Ni *fcc*	Ni *hcp*	Ni-back	First *h*-BN	Second h-BN	First graphene Total	First graphene Partial C1/C2	Second graphene Total	Second graphene Partial C1/C2
Monolayer graphene/ monolayer *h*-BN/Ni	N-*top*:B-*fcc*	*fcc*:*hcp*	0.5181 (0.0332)	0.5585 (0.0021)	0.5187 (0.0105)	0.6070 (−0.0284)	0.0106 (−0.0288)	…	−0.0066 (−0.0146)	−0.0075/0.0009 (−0.1238/0.1092)	…	…
Monolayer graphene/ bilayer *h*-BN/Ni	N-*top*:B-*fcc* B-*top*:*N*-*hcp*	*top*:*fcc*	0.5188 (0.0350)	0.5640 (0.0019)	0.5250 (0.0071)	0.6000 (−0.0264)	0.0115 (−0.0335)	−0.0012 (0.0010)	−0.0187 (−0.0092)	−0.0027/−0.0160 (0.1123/−0.1215)	…	…
Monolayer graphene/ bilayer *h*-BN/Ni	N-*top*:B-*fcc* B-*hcp*:*N*-*fcc*	*top*:*hcp*	0.5182 (0.0594)	0.5583 (0.0023)	0.5130 (0.0090)	0.6003 (−0.0277)	0.0119 (−0.0593)	−0.0014 (0.0)	−0.0159 (−0.0110)	−0.0130/−0.0029 (−0.1236/0.1126)	…	…
Monolayer graphene/ bilayer *h*-BN/Ni	N-*top*:B-*fcc* B-*top*:*N*-*fcc*	*top*:*hcp*	0.5198 (0.0408)	0.5685 (0.0050)	0.5291 (0.0085)	0.6054 (−0.0254)	0.0109 (−0.0417)	−0.0059 (−0.0009)	−0.0231 (−0.0059)	−0.0068/−0.0163 (0.1043/−0.1102)	…	…
Bilayer graphene/ bilayer *h*-BN/Ni	N-*top*:B-*fcc* B-*hcp*:*N*-*fcc*	*top*:*hcp* *top*:*fcc*	0.5269 (0.0586)	0.5613 (0.0049)	0.5188 (0.0091)	0.5987 (0.0276)	0.0110 (−0.0599)	−0.0002 (0.0011)	−0.0018 (−0.0107)	−0.0015/−0.0003 (−0.1121/0.1119)	−0.0254 (−0.0002)	−0.0207/−0.0047 (−0.1242/0.1135)
Bilayer graphene/ bilayer *h*-BN/Ni	N-*top*:B-*fcc* B-*top*:*N*-*hcp*	*top*:*fcc* *hcp*:*fcc*	0.5112 (0.0609)	0.5580 (0.0019)	0.5167 (0.0097)	0.6035 (−0.0248)	0.0124 (−0.0638)	0.0026 (−0.0050)	0.0023 (−0.0017)	0.0000/0.0023 (0.1140/−0.1157)	−0.0077 (0.0005)	−0.0036/−0.0041 (0.1145/−0.1140)
Bilayer graphene/ bilayer *h*-BN/Ni	N-*top*:B-*fcc* B-*top*:*N*-*fcc*	*top*:*hcp* *top*:*fcc*	0.51380 (0.0448)	0.5577 (−0.0028)	0.5370 (0.0098)	0.5975 (−0.0291)	−0.0154 (−0.0437)	−0.0042 (0.0004)	−0.0110 (−0.0070)	−0.0082/−0.0028 (0.1080/(−0.0115)	−0.0149 (0.0014)	−0.0049/−0.0100 (−0.1125/0.1139)

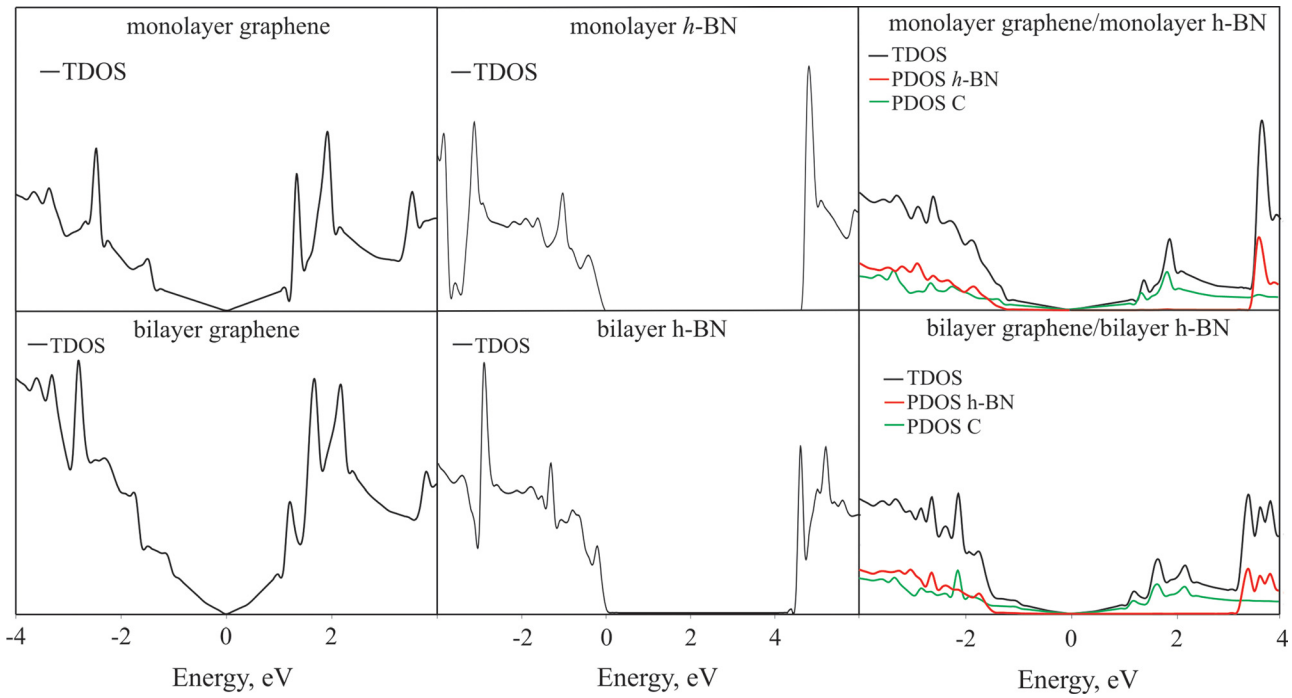

FIG. 2. Total (black lines) and partial (red for *h*-BN and green for graphene) density of states of monolayer and bilayer graphene (left), monolayer and bilayer *h*-BN (middle) and monolayer graphene/monolayer *h*-BN, and bilayer graphene/bilayer *h*-BN (right).

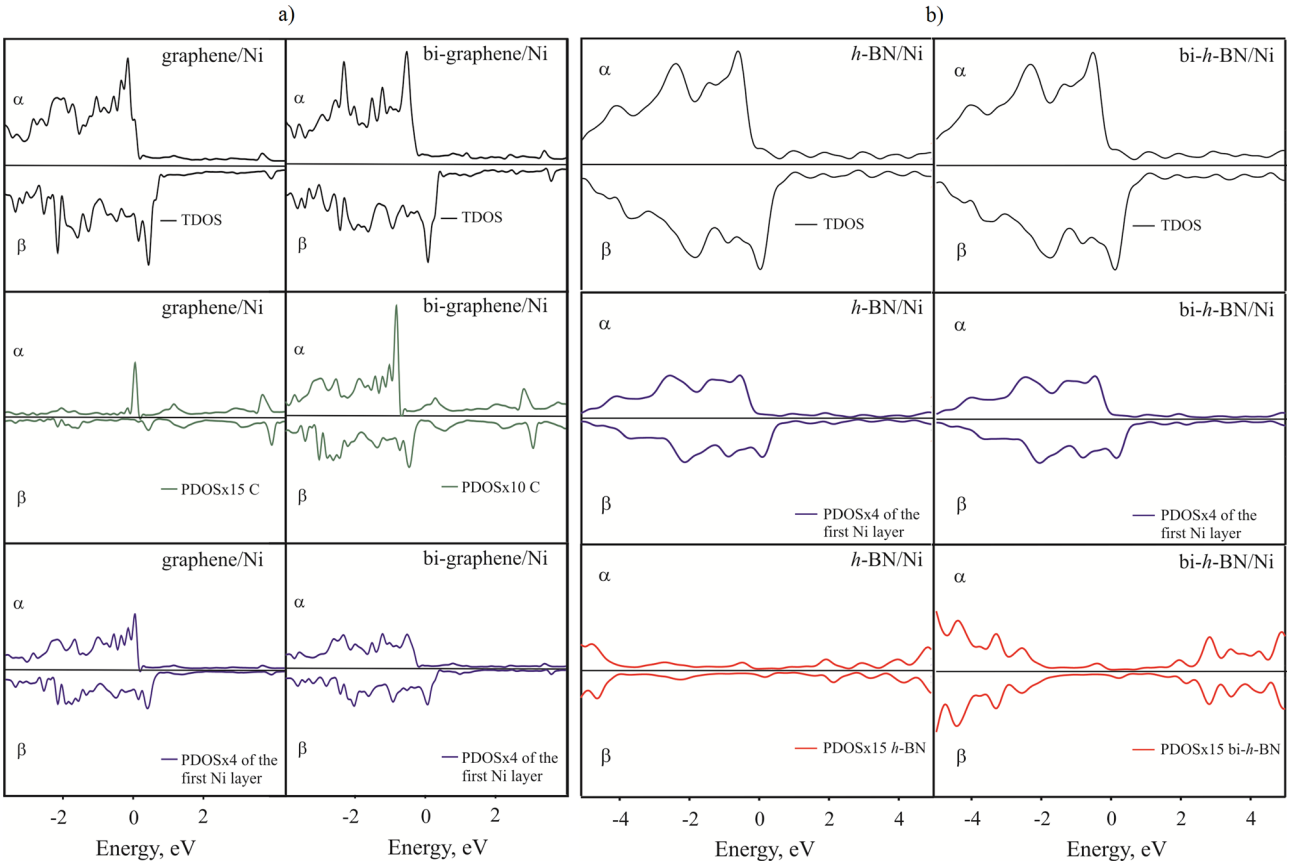

FIG. 3. (a) Total (black lines) and partial (dark blue for the first (top) Ni layer and green for graphene) density of states of monolayer graphene/Ni (left) and bilayer graphene/Ni (AB) (right) composites. (b) Total (black lines) and partial density of states (red for *h*-BN) of monolayer *h*-BN/Ni (left) and bilayer *h*-BN/Ni (AB) (right) composites. The PDOS of the graphene, *h*-BN, and Ni fragments were multiplied by factors 15, 15, and 4, respectively.

Typical density of states of the graphene/*h*-BN/Ni nanocomposites are presented in Fig. 4. The TDOS is mainly determined by the Ni fragment for all samples. The energy splitting of both spin-up and spin-down main peaks are close to binary systems and approximately equal to 0.5-0.6 eV. The presence of Ni fragment leads to strong asymmetry of spin-up and spin-down states in wide energy region from −4 up to 3 eV due to hybridization of Ni and *h*-BN electronic states.

Hybridization of the graphene and *h*-BN electronic states with Ni states in the vicinity of Fermi level can be revealed by comparison of the TDOSs of free-standing graphene and *h*-BN (Fig. 2) with graphene and *h*-BN partial DOSs of graphene/Ni(111) (Fig. 3(a)) and *h*-BN/Ni(111) (Fig. 3(b)) composites. One can clearly see pronounced reshape and limited hybridization of both spin-up and spin-down states due to interactions between the fragments. For graphene/Ni(111) composites, the hybridization occurs at −0.1 eV and +0.5 eV for spin-up and spin-down states, respectively. For the *h*-BN/Ni(111) composite, the hybridization of the states is more pronounced and take place in the energy region from −3 up to 3 eV. The chemical interactions of the fragments lead to redistributing of the *h*-BN states into the vicinity of Fermi level with their participation in formation of metallic states of the composites. Due to complex and metallic nature of electronic structure of the composites in the vicinity of the Fermi level, the band structure in this energy region is informative and cannot be clearly analyzed.

The spin polarization of graphene fragment without direct chemical interactions with the Ni plate can be interpreted in terms of the effective size of exchange-correlation holes (Wigner-Seitz radius, WSR) of B, C, N, and Ni elements (Table IX). Even in the simplest form,[43] WSRs are comparable with interatomic distances. Radius of the exchange-correlation hole obtained through LDA provides an estimate of the spatial extent of the true exchange-correlation hole. For all metals investigated in Ref. 44, this approximate exchange-correlation hole radius is comparable to the distance separating neighboring atoms. The sum of the WSR for Ni and C (3.781 Å + 4.631 Å = 8.412 Å) is comparable with or even greater than the distances between the first Ni layer and internal/external graphene fragments (from 5.345 up to 11.945 Å for the thickest bilayer graphene/bilayer *h*-BN/Ni nanocomposite, Table V). The comparable sizes of the sum of the WSRs and total thickness of the graphene and *h*-BN parts cause the direct exchange interactions of the nickel- and graphene-localized states and induce a significant degree of spin polarization of all fragments in the nanocomposites.

In summary, the atomic and electronic structure of the Ni plate, a set of the graphene and *h*-BN structures, graphene/Ni, *h*-BN/Ni, and graphene/*h*-BN/Ni nanocomposites with different number of graphene and *h*-BN layers and in

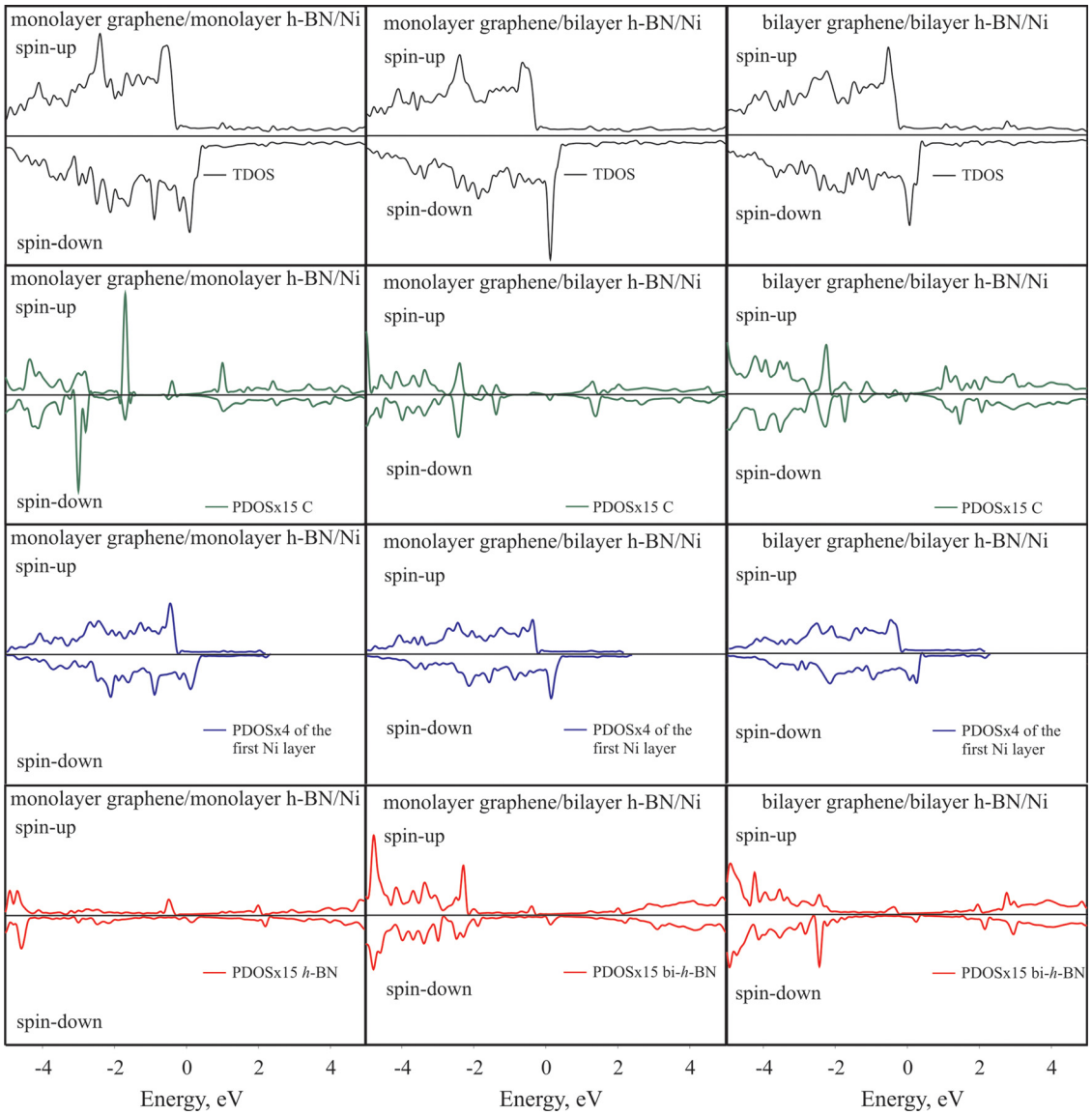

FIG. 4. Total (black lines) and partial (red for *h*-BN, dark blue for the first (top) Ni plate, and green for graphene) density of states of monolayer graphene/monolayer *h*-BN/Ni (top), monolayer graphene/bilayer *h*-BN/Ni (middle), and bilayer graphene/bilayer *h*-BN/Ni (b) composites. The PDOS of the graphene, *h*-BN, and Ni fragments were multiplied by factors 15, 15, and 4, respectively. The h-BN and graphene fragments are in (AB) type of mutual configurations.

different mutual arrangements were studied using LDA/PW/PP/PBC calculations. It was shown that the C-*top*:C-*fcc* and N-*top*:B-*fcc* types of the graphene/Ni and *h*-BN/Ni interfaces are energetically favorable. The interface formation of *h*-BN and graphene with the Ni(111) surface leads to strong energy shifts of spin-up and spin-down states and considerable redistribution of the density of states peak intensities. The spin polarization of graphene on Ni and on *h*-BN/Ni is caused by direct electronic exchange interactions of spin polarized Ni with graphene states even through multilayer *h*-BN media.

TABLE IX. The LDA exchange-correlation hole effective sizes, in Å unit.

Atom	Effective size	Reference
B	4.253	theory,[45] exp.[46]
C	3.781	theory,[45] exp.[46]
N	2.683	theory,[45] exp.[46]
Ni	4.631	theory,[45] exp.[46]

ACKNOWLEDGMENTS

This work was supported by JAEA Research fellowship (P.V.A.). P.V.A. also acknowledges JAEA ASRC and Molecular Spintronics Group for hospitality and fruitful collaboration. The authors are grateful to the ICS SB RAS and SFU CC (Krasnoyarsk), ISC RAS and MSU CRC, (SKIF MSU "Chebyshev", Moscow) for computer resources. This work was partially supported by the RFBR grant 12-02-31417.

[1]C. H. Marrows and B. J. Hickey, Philos. Trans. R. Soc. A **369**, 3027 (2011).
[2]W. J. M. Naber, S. Faez, and W. G. van derWiel, J. Phys. D: Appl. Phys. **40**, R205 (2007).
[3]M. Shiraishi and T. Ikoma, Physica E **43**, 1295 (2011).

[4]N. Tombros, C. Jozsa, M. Popinciuc, H. T. Jonkman, and B. J. van Wees, Nature **448**, 571 (2007).
[5]S. J. Chae, F. Günes, K. K. Kim, E. S. Kim, G. H. Han, S. M. Kim, H.-J. Shin, S.-M. Yoon, J.-Y. Choi, M. H. Park, C. W. Yang, D. Pribat, and Y. H. Lee, Adv. Mater. **21**, 2328 (2009).
[6]Yu. S. Dedkov and M. Fonin, New J. Phys. **12**, 125004 (2010).
[7]M. Weser, Y. Rehder, K. Horn, M. Sicot, M. Fonin, A. B. Preobrajenski, E. N. Voloshina, E. Goering, and Yu. S. Dedkov, Appl. Phys. Lett. **96**, 012504 (2010).
[8]M. Weser, E. N. Voloshina, K. Horna, and Yu. S. Dedkov, Phys. Chem. Chem. Phys. **13**, 7534 (2011).
[9]E. N. Voloshina, A. Generalov, M. Weser, S. Böttcher, K. Horn, and Yu. S. Dedkov, New J. Phys. **13**, 113028 (2011).
[10]R. Rosei, M. Decrescenzi, F. Sette, C. Quaresima, A. Savoia, and P. Perfetti, Phys. Rev. B **28**, 1161 (1983).
[11]Y. Gamo, A. Nagashima, M. Wakabayashi, M. Terai, and C. Oshima, Surf. Sci. **374**, 61 (1997).
[12]G. Bertoni, L. Calmels, A. Altibelli, and V. Serin, Phys. Rev. B **71**, 075402 (2005).
[13]G. Kalibaeva, R. Vuilleumier, S. Meloni, A. Alavi, G. Ciccotti, and R. Rosei, J. Phys. Chem. B **110**, 3638 (2006).
[14]L. Adamska, Y. Lin, A. J. Ross, M. Batzill, and I. I. Oleynik, Phys. Rev. B **85**, 195443 (2012).
[15]W. Auwärter, M. Muntwiler, J. Osterwalder, and T. Greber, Surf. Sci. **545**, L735 (2003).
[16]M. Muntwiler, W. Auwärter, F. Baumberger, M. Hoesch, T. Greber, and J. Osterwalder, Surf. Sci. **472**, 125 (2001).
[17]W. Auwärter, T. J. Kreutz, T. Greber, and J. Osterwalder, Surf. Sci. **429**, 229 (1999).
[18]J. Osterwalder, W. Auwärter, M. Muntwiler, and T. Greber, e-J. Surf. Sci. Nanotechnol. **1**, 124 (2003).
[19]T. Greber, W. Autwärter, M. Hoesch, G. Grad, P. Blaha, and J. Osterwalder, Surf. Rev. Lett. **9**, 1243 (2002).
[20]A. B. Preobrajenski, A. S. Vinogradov, and N. Mårtensson, Phys. Rev. B **70**, 165404 (2004).
[21]A. Nagashima, N. Tejima, Y. Gamou, T. Kawai, and C. Oshima, Phys. Rev. Lett. **75**, 3918 (1995).
[22]A. Nagashima, N. Tejima, Y. Gamou, T. Kawai, and C. Oshima, Phys. Rev. B **51**, 4606 (1995).
[23]G. B. Grad, P. Blaha, K. Schwarz, W. Auwärter, and T. Greber, Phys. Rev. B **68**, 085404 (2003).
[24]J. G. Che, and H.-P. Cheng, Phys. Rev. B **72**, 115436 (2005).
[25]M. N. Huda and L. Kleinman, Phys. Rev. B **74**, 075418 (2006).
[26]J. Xue, J. Sanchez-Yamagishi, D. Bulmash, P. Jacquod, A. Deshpande, K. Watanabe, T. Taniguchi, P. Jarillo-Herrero, and B. J. LeRoy, Nature Mater. **10**, 282 (2011).
[27]G. Giovannetti, P. A. Khomyakov, G. Brocks, P. J. Kelly, and J. van den Brink, Phys. Rev. B **76**, 073103 (2007).
[28]J. Sławińska, I. Zasada, and Z. Klusek, Phys. Rev. **81**, 155433 (2010).
[29]G. Kresse and J. Hafner, Phys. Rev. B **49**, 14251 (1994).
[30]G. Kresse and J. Furthmuller, Phys. Rev. B **54**, 11169 (1996).
[31]H. J. Monkhorst and J. D. Pack, Phys. Rev. B **13**, 5188 (1976).
[32]P. Trucano and R. Chen, Nature **258**, 136 (1975).
[33]M. F. Craciun, S. Russo, M. Yamamoto, J. B. Oostinga, A. F. Morpurgo, and S. Tarucha, Nat. Nanotechnol. **4**, 383 (2009).
[34]C.-J. Shih, A. Vijayaraghavan, R. Krishnan, R. Sharma, J.-H. Han, M.-H. Ham, Z. Jin, S. Lin, G. L. C. Paulus, N. F. Reuel, Q. H. Wang, D. Blankschtein, and M. S. Strano, Nat. Nanotechnol. **6**, 439 (2011).
[35]C. H. Lui, Z. Li, K. F. Mak, E. Cappelluti, and T. F. Heinz, Nat. Phys. **7**, 944 (2011).
[36]P. V. Avramov, S. Sakai, S. Entani, Y. Matsumoto, and H. Naramoto, Chem. Phys. Lett. **508**, 86 (2011).
[37]V. L. Solozhenko, G. Will, and F. Elf, Solid State Commun. **96**, 1 (1995).
[38]P. K. Lam, R. M. Wentzcovitch, and M. L. Cohen, in *Synthesis and Properties of Boron Nitride*, Materials Science Forum Vol. 54 and 55, edited by J. J. Pouch and S. A. Alterovitz (Trans Tech, Zürich, Switzerland, 1990), pp. 165–192.
[39]N. Marom, J. Bernstein, J. Garel, A. Tkatchenko, E. Joselevich, L. Kronik, and O. Hod, Phys. Rev. Lett. **105**, 046801 (2010).
[40]A. Taylor, J. Inst. Met. **77**, 585 (1950).
[41]C. R. Dean, A. F. Young, I. Meric, C. Lee, L. Wang, S. Sorgenfrei, K. Watanabe, T. Taniguchi, P. Kim, K. L. Shepard, and J. Hone, Nat. Nanotechnol. **5**, 722 (2010).
[42]S. Masubuchi, K. Iguchi, T. Yamaguchi, M. Onuki, M. Arai, K. Watanabe, T. Taniguchi, and T. Machida, Phys. Rev. Lett. **109**, 036601 (2012).
[43]R. M. Martin, *Electronic Structure. Basic Theory and Practical Methods* (Cambridge University Press, 2004).
[44]A. van de Walle and G. Ceder, Phys. Rev. B **59**, 14992 (1999).
[45]U. Yxklinten, J. Hartford, and T. Holmquist, Phys. Scr. **55**, 499 (1997).
[46]Compiled by P. Eckerh and H. Kandler, in *Landolt-Bomstein, Numerical Data and Functional Relationships in Science and Technology*, edited by K.-H. Hellwege (Springer-Verlag, 1971).